Introduction

Reservoir fluids consist of complex mixtures of hydrocarbons and nonhydrocarbons existing at high pressure and temperature conditions, making it nearly impossible to fully describe their chemical structure. Depleted after years of production, the light-oil reservoir at hand is analyzed as a candidate for enhanced oil recovery (EOR). Several experiments have been conducted to characterize the reservoir fluid, including compositional analysis, plus fraction gas-oil ratio and molecular weight properties, constant mass expansion (CME), swelling tests with CO_2, and unswollen reservoir fluid viscosity. The objective of this project is to create a PVT-laboratory simulator that accurately reproduces available experimental data, and predicts other PVT fluid properties and phase behavior. This comprised of several steps, including expansion and lumping of components, tuning, CME, differential liberation (DLE), oil-phase viscosity, and pressure-temperature (PT) envelop construction.

Methodology and Implementation

This section outlines the major algorithms within the PVT simulator and finally provide tips on how to run the attached *ipynb* file and output results on Jupyter Notebook.

The Peng Robinson (PR) is the EOS of choice in this work. Critical temperature (T_c), critical pressure (P_c), acentric factor (ω), molecular weight (MW), and volume shift factor (c) are major EOS input parameters for each component of the mixture. Fluid components were lumped into a smaller number of pseudocomponents (PS) to form to cases: PS20 and PS10 (20 and 10 pseudocomponents, respectively). Following the Pederson et al. (2004) approach, the light oil components were expanded and lumped to have PS20 and PS10 seen in **Tables 1 and 2**. Note that lumping the lighter components was avoided as much as possible to emphasize their importance as the mixture at hand is light. In addition, expanding and lumping of the heavy-end components was done to have nearly equal mass fraction (~10%) in the PS20 case. Meanwhile, it was found that having roughly equal mass fraction (~39%) of the heavy-end PS away from C_{7-9} gives more accurate results in the PS10 case compared to the experimental data, so it is adapted.

As outlined in Chapter 6 of ENERGY 251 Notebook, flash calculations were performed using the Wilson equation to generate a first K_i-value guess and applying the Rachford-Rice equation with mixed bisection-Newton Raphson iterations to obtain the liquid fraction. The PR EOS is then applied to find the liquid and vapor compressibility factor roots (numerically or analytically) based

on minimum free Gibb's energy, molar volumes, and component fugacities. K_i-values were then updated for each iteration, until the system equilibrium is reached where $\widehat{f_i^l} = \widehat{f_i^v}$ for each component i = 1,2, … N_c. CME is implemented to find the bubble point pressure at any given temperature, i.e. 99° C, and eventually to construct the bubble point line of the PT diagram. An initial pressure guess was chosen to be within the two-phase envelop where flash calculations result in an initial liquid fraction. Pressure is then increased using Newton-Raphson and bisection to get liquid fraction ~1.0, where the pressure increments using Newton-Raphson are based on numerically calculated errors in $\sum_i^n$ zi ki $- 1 = 0$. Another routine similarly constructs the dew point line, but rather fixes a pressure value within the envelop and iterates over temperature to get liquid fraction of ~0.0 with based on errors in $\sum_i^n \mathrm{zi/ki} - 1 = 0$.

Table 1. PS20 EOS Input Parameters

PS	z	wt	Tc	Pc	ω	MW
	%	%	K	MPa		g/mol
CO2	0.32	0.09	304.2	7.39	0.228	44.0
N2	0.04	0.01	126.2	3.40	0.040	28.0
C1	15.65	1.53	190.6	4.60	0.008	16.0
C2	4.13	0.75	305.4	4.88	0.098	30.1
C3	4.02	1.08	369.8	4.25	0.152	44.1
iC4	1.01	0.36	408.1	3.65	0.176	58.1
nC4	2.85	1.01	425.2	3.80	0.193	58.1
iC5	1.53	0.67	460.4	3.38	0.227	72.2
nC5	1.76	0.77	469.6	3.37	0.251	72.2
C6	2.87	1.47	507.4	2.97	0.296	84.0
C7	6.66	3.89	548.7	2.74	0.333	96.0
C8	8.12	5.28	566.4	2.67	0.382	107.0
C9	7.21	5.30	585.2	2.55	0.444	121.0
C10-13	12.75	12.05	627.1	2.25	0.598	155.5
C14-17	9.04	11.62	685.8	1.89	0.825	211.5
C18-22	7.70	12.80	745.0	1.64	1.057	273.6
C23-27	5.01	10.46	806.0	1.47	1.277	343.6
C28-34	4.22	10.90	873.4	1.35	1.453	425.2
C35-45	3.13	10.34	966.2	1.23	1.484	544.1
C46-200	1.99	9.61	1166.6	1.10	0.634	796.0

Table 2. PS10 EOS Input Parameters						
PS	z	wt	Tc	Pc	ω	MW
	%	%	K	MPa		g/mol
CO2	0.32	0.09	304.2	7.39	0.228	44.0
N2-C1	15.69	1.53	190.4	4.60	0.008	16.1
C2	4.13	0.75	305.4	4.88	0.098	30.1
C3	4.02	1.08	369.8	4.25	0.152	44.1
iC4-nC4	3.86	1.36	420.7	3.76	0.189	58.1
iC5-nC5	3.29	1.44	465.3	3.37	0.240	72.2
C6	2.87	1.47	507.4	2.97	0.296	84.0
C7-9	21.99	14.47	568.5	2.64	0.392	108.3
C10-23	30.67	38.77	692.9	1.89	0.853	207.9
C24-200	13.16	39.04	957.4	1.28	1.227	488.0

Volume shifts were applied to the PR output volume as outlined by Jhaveri et al. (1988) where the heavier components are approximated as alkanes with d = 2.258 and e = 0.1823 to calculate the corresponding shift parameter S_i. The EOS was then tuned, which will be discussed in the following sections. DLE routine is also developed to simulate the change in oil formation volume factor (B_o), gas formation volume factor (B_g), and solution gas-oil ratio (R_s) at 99° C. Finally, mixture viscosity was calculated using the corresponding state approach with CH_4 as the reference substance. Meanwhile, the CH_4 viscosity at the reference temperature and reference density was estimated using the correlation of Hanley et al. (1975).

To run the algorithm, open the attached *ipynb* file in Jupyter Notebook. Click on the 'Kernel' tab. Choose 'Restart & Run All' to restart your kernel and run all the lines in order. All output results and plots will be displayed just below each corresponding line accordingly. All results incorporate volume translation and kij tuning effects.

Results

This section will briefly provide the major results and provide the relevant tables and figures. Discussion of the results will be provided in the following section.

PS20 and PS10 EOS input parameters are used through CME to calculate the saturation pressure and volumetrics with volume shifts, as seen in **Figs. 1 and 2**. PS10 was then tuned to match the saturation pressure and volumetrics through adjusting kij between CH_4-N_2 and the heavy hydrocarbons (C_{7-9}, C_{10-23}, C_{24-200}). Initial kij value choices were based on the correlation of Kordas et al. (1995) for PR, which results in negative kij values, seen in **Table 3**. To closely match the

experimental data, kij values were adjusted further to be more negative, seen in Table 3 and **Figs. 3 and 4**. Meanwhile, MW of the heavy components were adjusted up to 10%, yet their effect was not as significant compared to kij, so turning was limited to the latter. The modest effect of MW tuning is anticipated as the fluid at hand is an oil mixture which is generally less sensitive to MW adjustments compared to, for instance, gas condensate (Pederson et al. 1989).

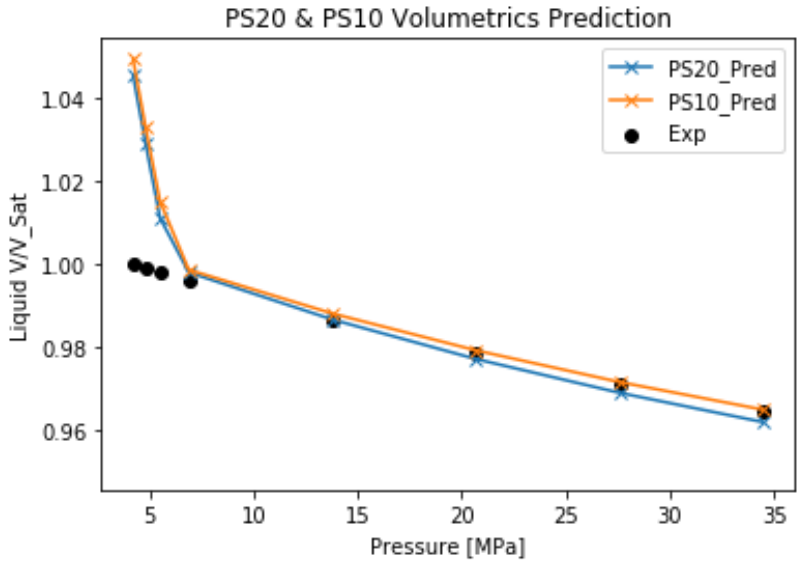

Fig. 1—V/V_sat plot against pressure of the PS20 and PS10 groups versus the experimental data after applying volume shifts and before tuning the binary interaction coefficients.

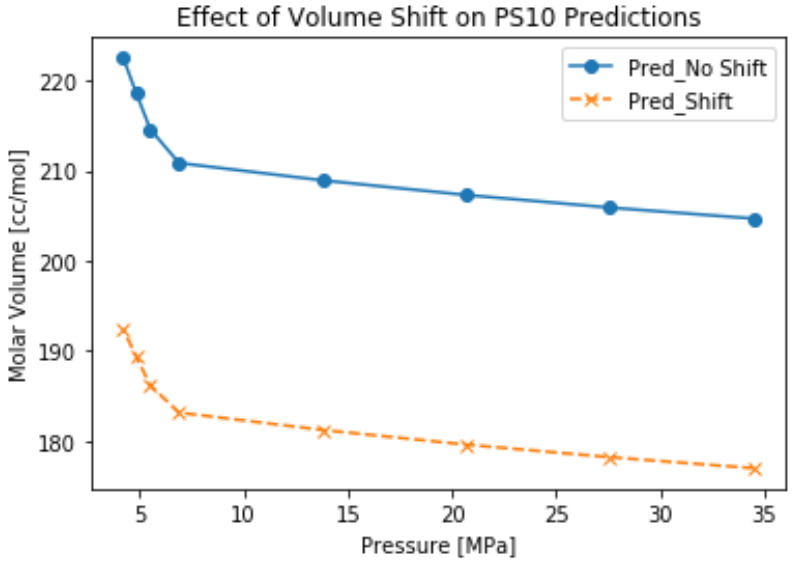

Fig. 2— Effect of volume shifts on the molar volume of PS10 as a function of pressure. The volume translation magnitude is about 30 cm^3/mol.

Table 3. Binary Interaction Coefficient Tuning				
PS (i)	PS (j)	Old kij	Kordas et al. Correlation	Final kij
CH4-N2	C7-9	0	-0.0054	-0.08
CH4-N2	C10-23	0	-0.0394	-0.18
CH4-N2	C24-200	0	-0.0553	-0.18

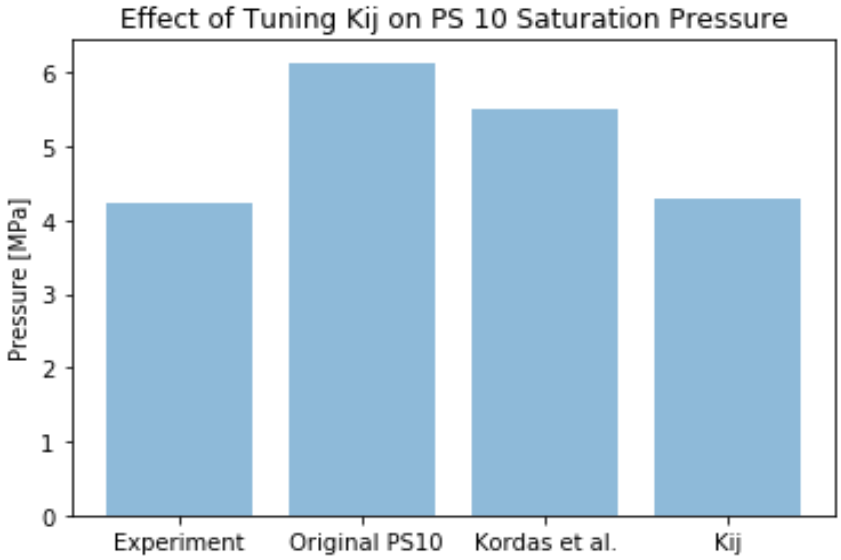

Fig. 3—Comparison of saturation pressure of the experimental data, non-tuned original PS10 case, tuned PS10 kij values with Kordas et al. (1995) correlation, and tuned PS10 with final kij values.

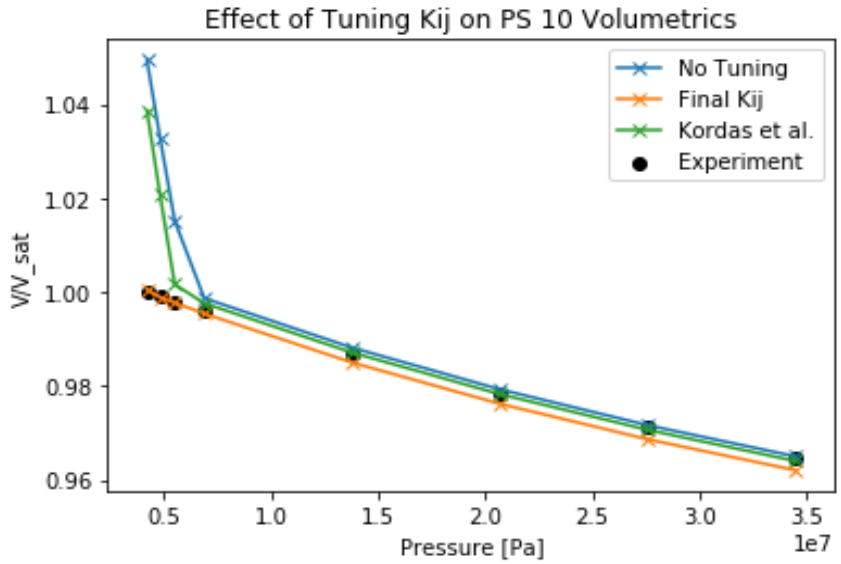

Fig. 4— V/V_sat plot against pressure to compare the effect of tuning kij on the prediction of the PS10 case versus the experimental data. The match is definitely better after tuning.

Using the discussed algorithms to calculate the bubble point line and dew point line, a PT diagram was constructed for the case of PS10. It is difficult to converge around the critical point, so the region in between is left out, seen in **Fig. 5**. DLE of the PS10 is performed in order to estimate B_o, B_g, and R_s as seen in **Figs. 6-8**. Mixture viscosity is then approximated using the corresponding states method with CH_4 as the reference substance. CH_4 density can be calculated using EOS and two options are examined: PR and Soave-Redlich-Kwong (SRK), seen in **Figs. 9 and 10**.

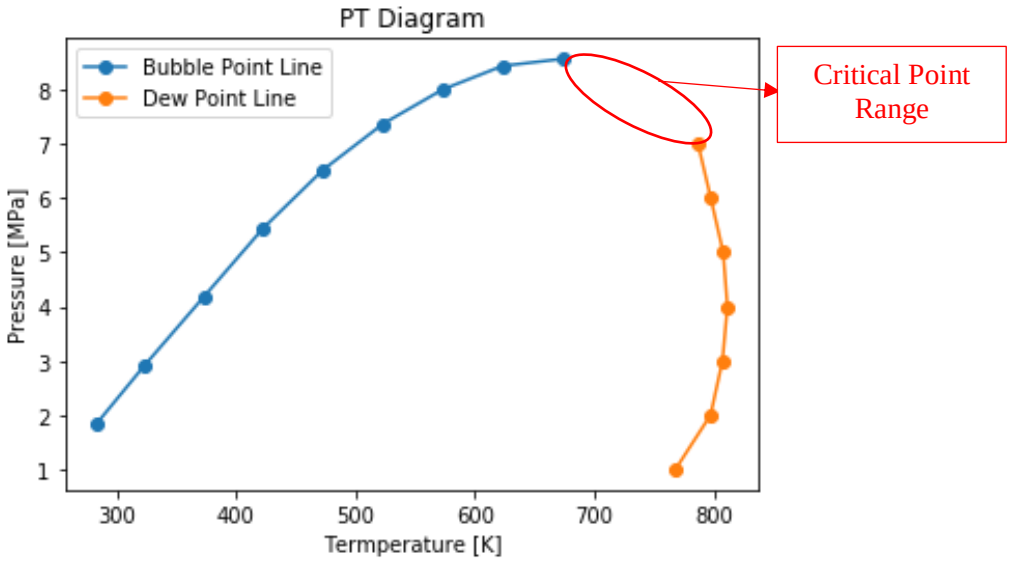

Fig. 5—PT diagram plotted for the tuned PS10 case highlighting the bubble point line, dew point line, and critical point range. The algorithms do not converge to correct values around the critical point range, but rather shoot up.

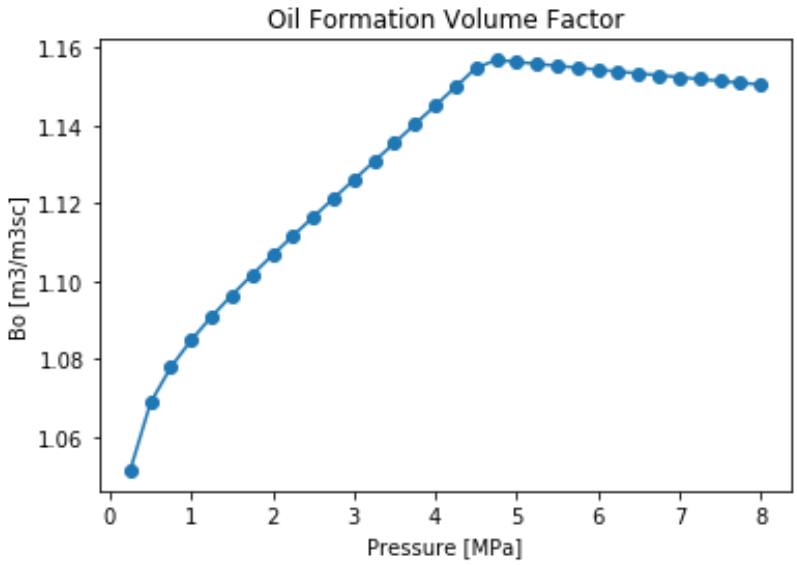

Fig. 6—Oil formation volume factor plot against pressure of the PS10 case. It is linearly increasing as pressure decreases above the bubble point and then it drops dramatically below the bubble point due to gas release.

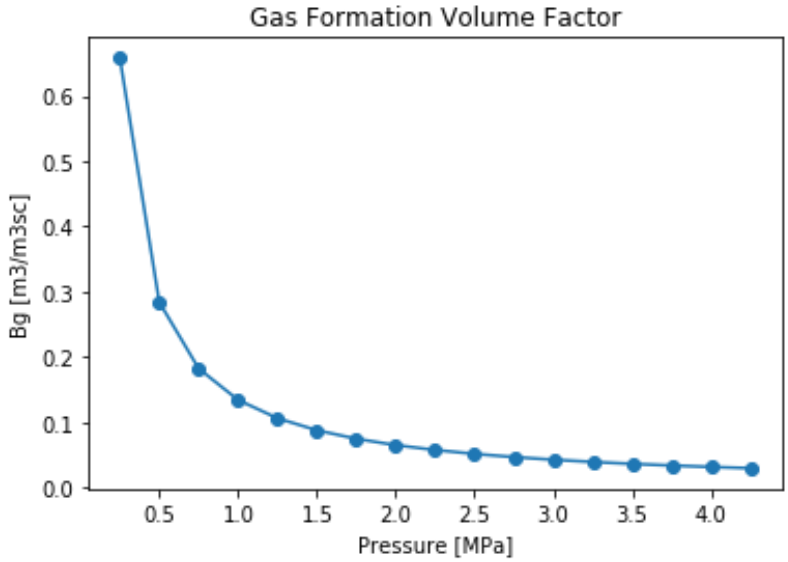

Fig. 7—Gas formation volume factor against pressure. Its values are zero above the bubble point pressure and it increases gradually as pressure is dropped below the bubble point and this rate becomes exponential as gas has high compressibility compared to liquid.

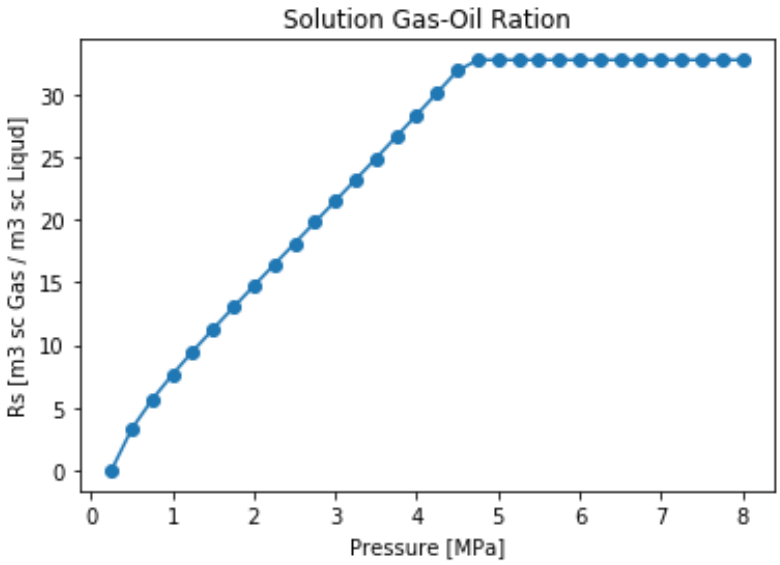

Fig. 8—Solution gas-oil ratio plotted against pressure with constant values above the bubble point pressure since the solution gas is not released. It then starts dropping linearly as the solution gas is released.

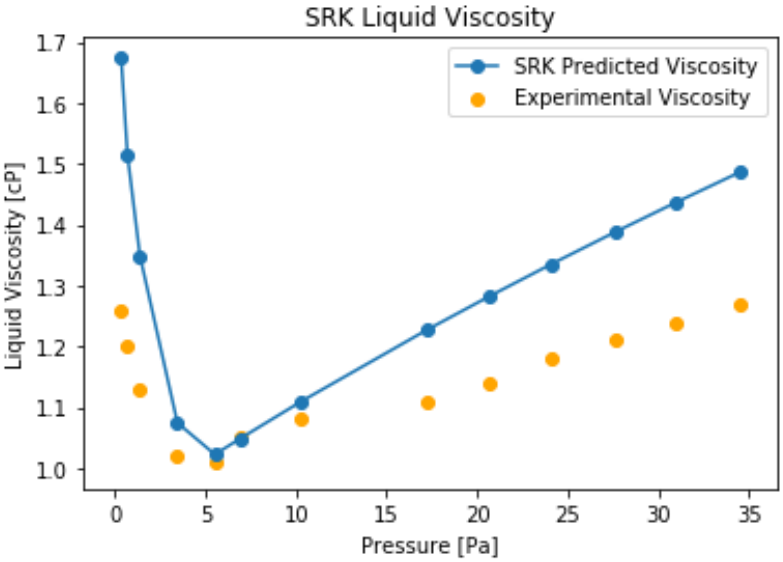

Fig. 9—Mixture viscosity plotted against pressure with excellent results as the CH_4 density is approximated using SRK. Note the trends are appropriate and the magnitudes are closest around the bubble point pressure.

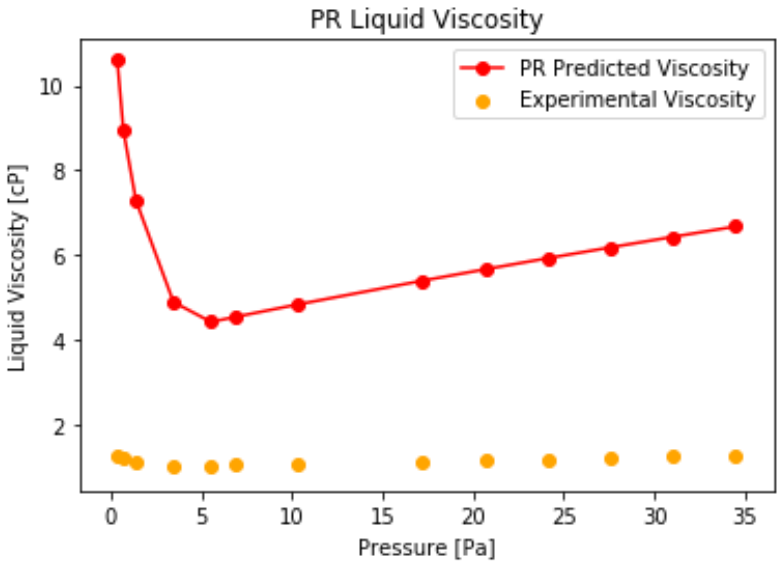

Fig. 10—Mixture viscosity plotted against pressure with a good trend but far values from the experimental data as the CH_4 density is approximated using PR.

Discussion

Figs. 1 and 2 show a molar volume shift of ~30 cc/mol in the PS10 case, and excellent match of both PS20 and PS10 to the experimental V/V_sat above the bubble point. Yet, both PS20 and PS10 predict a higher saturation pressure with a relative error of ~42%. This is due to underestimating the attractive forces between the different components where the intermolecular forces are predicted by PR EOS to be weaker, releasing gas at higher pressures and incurring error.

PS10 is tuned in this case but with the objective of only matching the experimental saturation pressure and volumetrics (it is also found to match viscosity data eventually). The Kordas et al. (1995) correlation is used to acquire initial estimation of the appropriate kij values for our case. Negative kij values are acquired which means that the intermolecular forces are indeed underestimated by setting kij to zero. Fateen et al. (2012) show that kij of N_2 and n-octane is -0.41 and Xu et al. (2015) point out that kij is temperature and pressure dependent. Meanwhile, the Kordas et al. (1995) correlation only accounts for the acentric factor of the heavy components interacting with CH_4. So, further tuning of kij values is applied to closely match the saturation pressure (relative error ~1.4%) and volumetrics, seen in Table 3 and Figs. 3 and 4.

The PT diagram, Fig. 5, shows reservoir fluid cricondenbar and cricondentherm of approximately 8.5 MPa and 830 K, respectively. With the high content of light components, this

reservoir is likely to deplete relatively fast and release large amounts of vapor as it falls below the bubble point. As gas volumes become sufficiently large, gas production increases and oil rates decline (Terry and Rogers 2014); hence, EOR operations are required.

To converge faster in the bubble point line Fig. 5, the algorithm starts at lower temperatures and each point would assume the previous bubble point pressure at the previous temperature iteration as its initial guess with 80% reduction factor to ensure it is still within the two-phase envelop. Similarly, the dew point curve was constructed starting at low pressure values and convergence was enhanced by taking 80% of the previous temperature as the initial guess for the following temperature which is again found to enhance the convergence rate. Meanwhile, converging around the critical point is found to be difficult using this approach as the parameters could correspond to a single solution, multiple solutions or no solutions (Michelsen 1980).

Fig. 6 shows B_o with 1.14-1.16 m^3/m^3sc and reasonable trends as it is increasing with decreasing pressure above the bubble point, then decreasing rapidly as the system drops below the bubble point as gas is released. Fig. 7 shows B_g trends of the reservoir fluid gas where it is extremely small at higher pressures just below the bubble point and eventually increases exponentially below 0.5 MPa as the system approaches standard conditions. Fig. 8 shows R_s with constant ration of 36 m^3 sc gas / m^3 sc liquid above the bubble point pressure as no bubbles have formed yet, and then it drops linearly below the bubble point pressure down to zero as the solution gas is continuously released.

To fully classify the reservoir at hand, PS10 case density is plotted, seen in **Fig. 11**. Note that the volume shifts decrease molar volume predictions and estimate higher intermolecular forces which translates into higher densities. Observing the range for major properties above the bubble point, seen in **Table 4**, we can classify the fluid at hand as black-oil category based on the property ranges provided by McCain (1994).

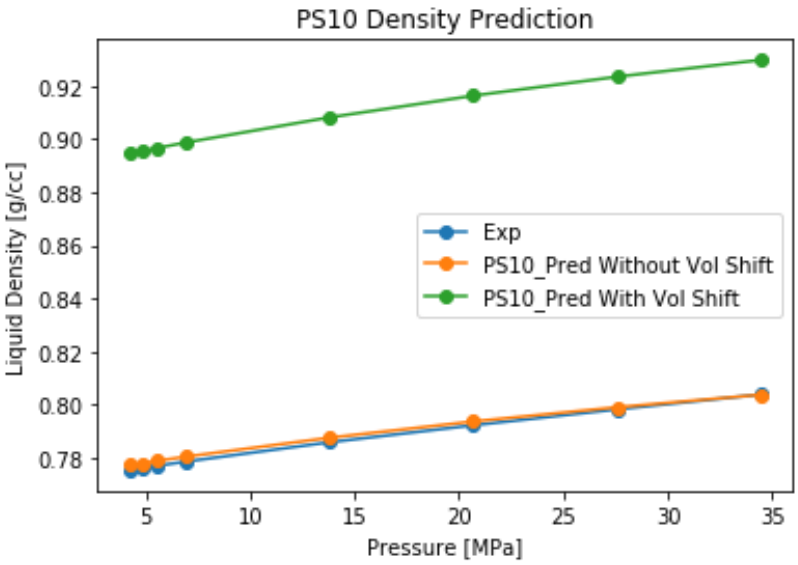

Fig. 11—Plot of liquid density predictions with and without volume shifts as compared with the experimental data. Note that the volume shifts push the density predictions away from the experimental data.

Table 4. Reservoir Oil Properties at Initial Conditions

Bo	Rs	MW	z_{C7+}	Density
m3/m3sc	m3 sc gas / m3 sc liquid	g/mol	Mole %	g/cc
1.14 - 1.16	36	164	65.82	0.89 - 0.93

SRK and PR EOS are used to estimate the reference substance, CH_4, which is then used to quantify the mixture viscosity, as seen in Figs 9 and 10. Both give similar trends where viscosity increases linearly with increasing pressure above the bubble point due to compression of particles. Meanwhile, viscosity shoots up rapidly as pressure decreases below the bubble point due to the release of dissolved gas. Hence, the minimum viscosity is at the saturation pressure. Moreover, SRK EOS yields a better match to the experimental data compared to PR EOS due to the different CH_4 density outputs at the reference temperature range of 60-111 K. This difference is justified by Mathies et al. (2014) who observed that the SRK EOS is superior to the PR EOS in predicting CH_4 density below the pseudo-boiling temperature of 111.5 K.

Summary

This work introduces a PVT-laboratory simulator to replicate given experimental data, and compute other PVT properties and reservoir fluid phase behavior. Routines were developed in

Python to lump components into PS20 and PS10 cases. Generally, having less pseudocomponents has the advantage of reducing the computational cost as long as it yields reasonable simulation results when compared with experimental data. The model is tuned to match the experimental saturation pressure and volumetrics through making educated, reasonable adjustments to kij values. The resulting magnitudes of density, Bo, Rs, MW, and others matched the typical ranges of a black oil. Finally, the choice of the recommended EOR technique will be dependent on multiple factor besides the reservoir fluid characteristics, including rock properties (permeability, porosity, lithology, depth, etc), residual oil saturation, etc.

Literature Cited

Fateen, S., Khalil, M., and Elnabawy, A. 2013. Semi-Empirical Correlation for Binary Interaction Parameters of the Peng–Robinson Equation of State with the Van Der Waals Mixing Rules for the Prediction of High-Pressure Vapor–Liquid Equilibrium. *Journal of Advanced Research*, **4**, 137-145.

Hanley, H., McCarty, R., and Haynes, W. 1975. Equations for the Viscosity and Thermal Conductivity Coefficients of Methane. *Cryogenics*, **15**(7), 413-417.

Jhaveri, B. and Youngren, G. 1988. Three-Parameter Modification of the Peng-Robinson Equation of State To Improve Volumetric Predictions. *SPE Reservoir Engineering*, **3**(03), 1-33.

Kordas, A., Magoulas, K., Stamataki, S., et al. 1995. Methane-Hydrocarbon Interaction Parameters Correlation for the Peng-Robinson and the t-mPR Equation of State. *Fluid Phase Equilibria*, **112**, 33-44.

McCain, W. 1994. Heavy Components Control Reservoir Fluid Behavior. *JPT*, **46**(09), 746-750.

Pederson K., Fredenslund, A., and Thomassen, P. 1989. *Prop. of Oils and Natural Gases*. Volume 5, Gulf Pub Co.

Pederson, K., Milter, J., and Sorensen, H. 2004. Cubic Equations of State Applied to HT/HP and Highly Aromatic Fluids. *SPE Journal*, **9**(02), 186-192.

Xu, X., Jaubert, J, Privat, R., et al. 2015. Predicting Binary-Interaction Parameters of Cubic Equations of State for Petroleum Fluids Containing Pseudo-Components. *Ind. Eng. Chem. Res.*, **54**, 2816-2824.